Supplementary information for:

Three-dimensional structure of a flavivirus dumbbell RNA reveals molecular details of an RNA regulator of replication

Benjamin M. Akiyama[1], Monica E. Graham[2], Zoe O′Donoghue[2], J. David Beckham[2,3], & Jeffrey S. Kieft[1,4*]

[1]Department of Biochemistry and Molecular Genetics, [2]Department of Immunology and Microbiology, [3]Department of Medicine Division of Infectious Diseases, and [4]RNA BioScience Initiative, University of Colorado Denver School of Medicine, Aurora, Colorado, 80045, USA

*To whom correspondence should be addressed: 303-724-3257; Jeffrey.Kieft@cuanschutz.edu

Table of Contents:

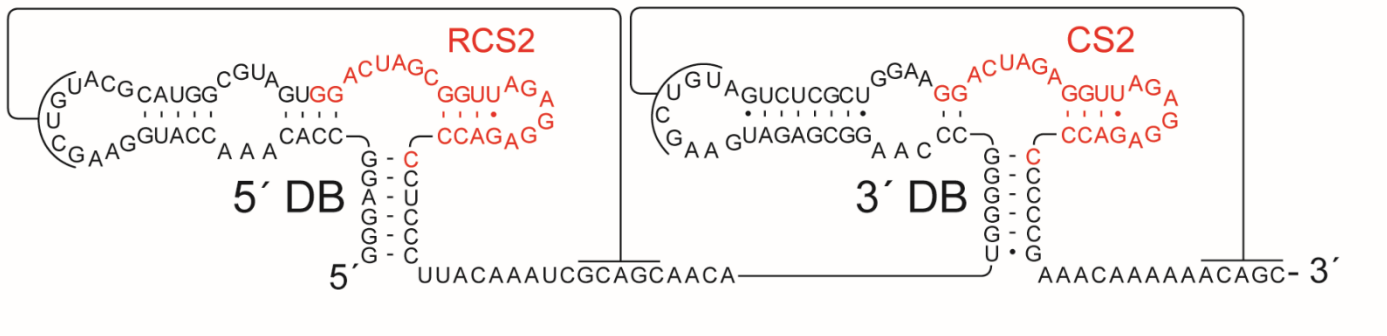

Suppl. Figure S1. Organization of RCS2 and CS2 motifs. Secondary structure diagram of DENV-2 (accession number NC_001474.2) dumbbell (DB) elements showing the 5′ and 3′ DBs. The locations of the RCS2 and CS2 motifs are highlighted in red. Lines denote the base-pairing that forms the putative pseudoknots.

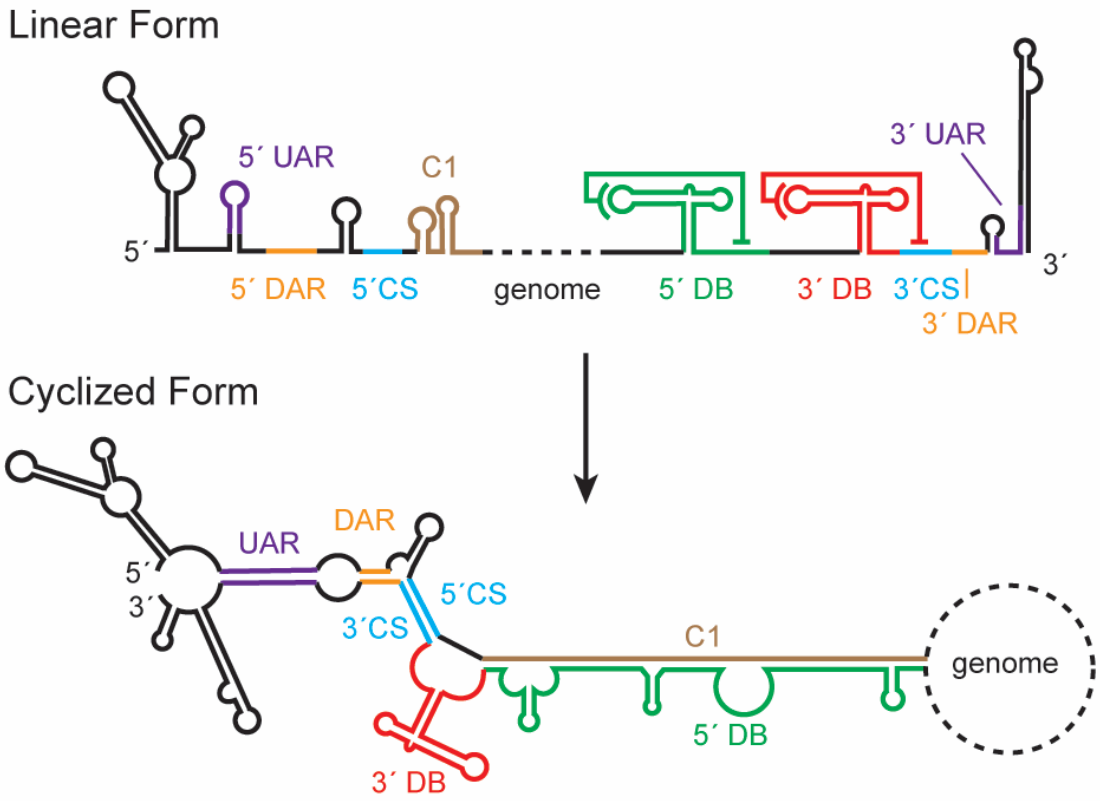

Suppl. Figure S2. Proposed genome rearrangements during viral cyclization based on predicted UTR secondary structures. The 3′ DB (red) pseudoknot unfolds during viral cyclization, exposing the 3′ CS for binding to the 5′ CS (cyan). 5′-3′ CS base pairing is supplemented by base pairing in the downstream of AUG region (DAR, orange) and upstream of AUG region (UAR, magenta). The 5′ DB (green) partially unfolds to base pair with the C1 region (brown). Figure derived from (1).

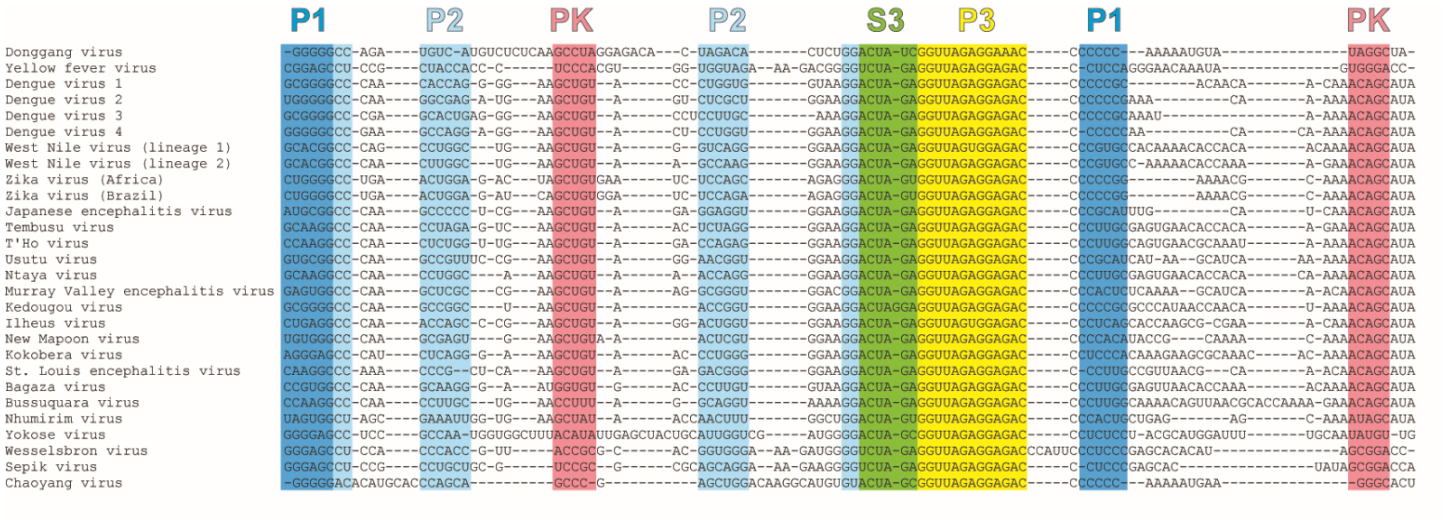

Suppl. Figure S3. Structural conservation of DONGV to other MBFVs. Sequence alignment of MBFV DB RNAs demonstrating sequence homology of DONGV to related MBFVs. Structure elements from the DONGV crystal structure are highlighted in the alignment and colored as in Figure 2.

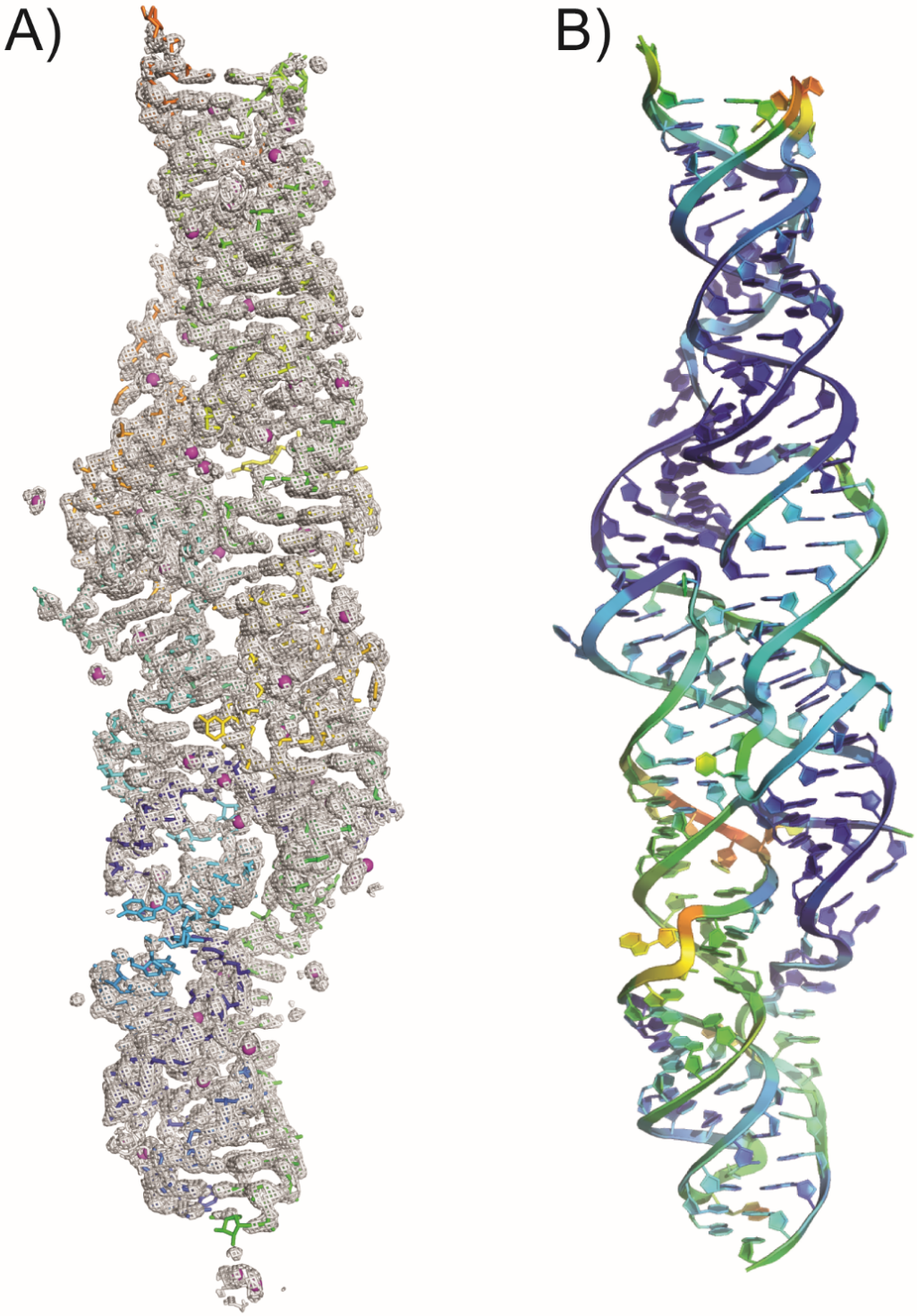

Suppl. Figure S4. Composite omit map and relative b-factors. A) Simulated annealing composite omit map of the asymmetric unit of the DONGV DB RNA crystal structure at a 1 σ cutoff compared with the three-dimensional structure model. Iridium atoms are shown as magenta spheres with amines omitted for clarity. **B)** The two copies of the RNA in the asymmetric unit colored by relative B-factors, red represents highest and blue represents lowest.

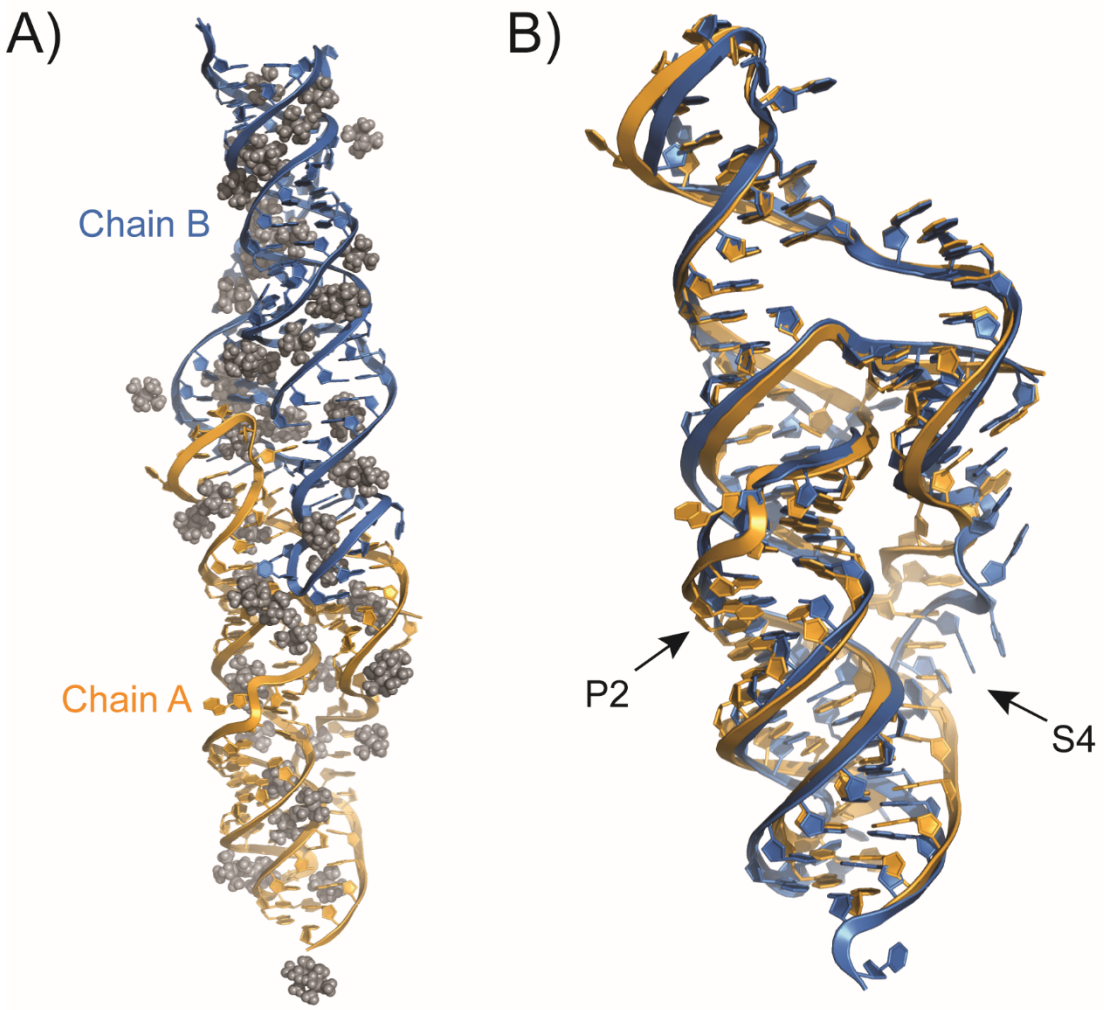

Suppl. Figure S5. Comparison of two molecules in the asymmetric unit. A) The final refined structure of the crystallographic asymmetric unit containing two copies of the RNA (blue and orange) with positions of bound iridium (III) hexammine shown in grey. **B)** Both copies of the RNA in the asymmetric unit are shown overlaid, with an overall RMSD of 2.3 Å (all atoms).

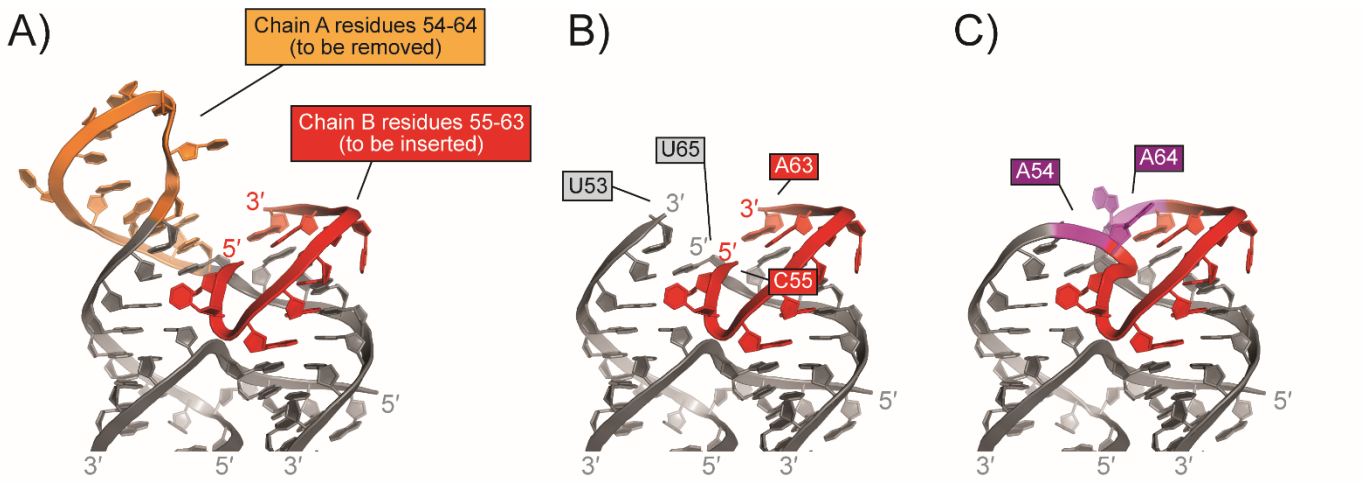

Suppl. Figure S6. Modeling of the monomeric solution structure. A) Given the observed base pairing between residues 57-60 and 67-70 *in trans*, we determined residues 55-63 from chain A (orange) could be replaced with residues 55-63 from chain B (red) to obtain a model of a solution structure of the DONGV DB RNA. **B)** Model of the monomeric structure of the DONGV DB lacking connecting residues A54 and A64. **C)** To complete the model, residues A54 and A64 (magenta) were inserted and energy minimized using Coot without electron density restraints in order to bridge U53 and U55 as well as G65 and A63 respectively.

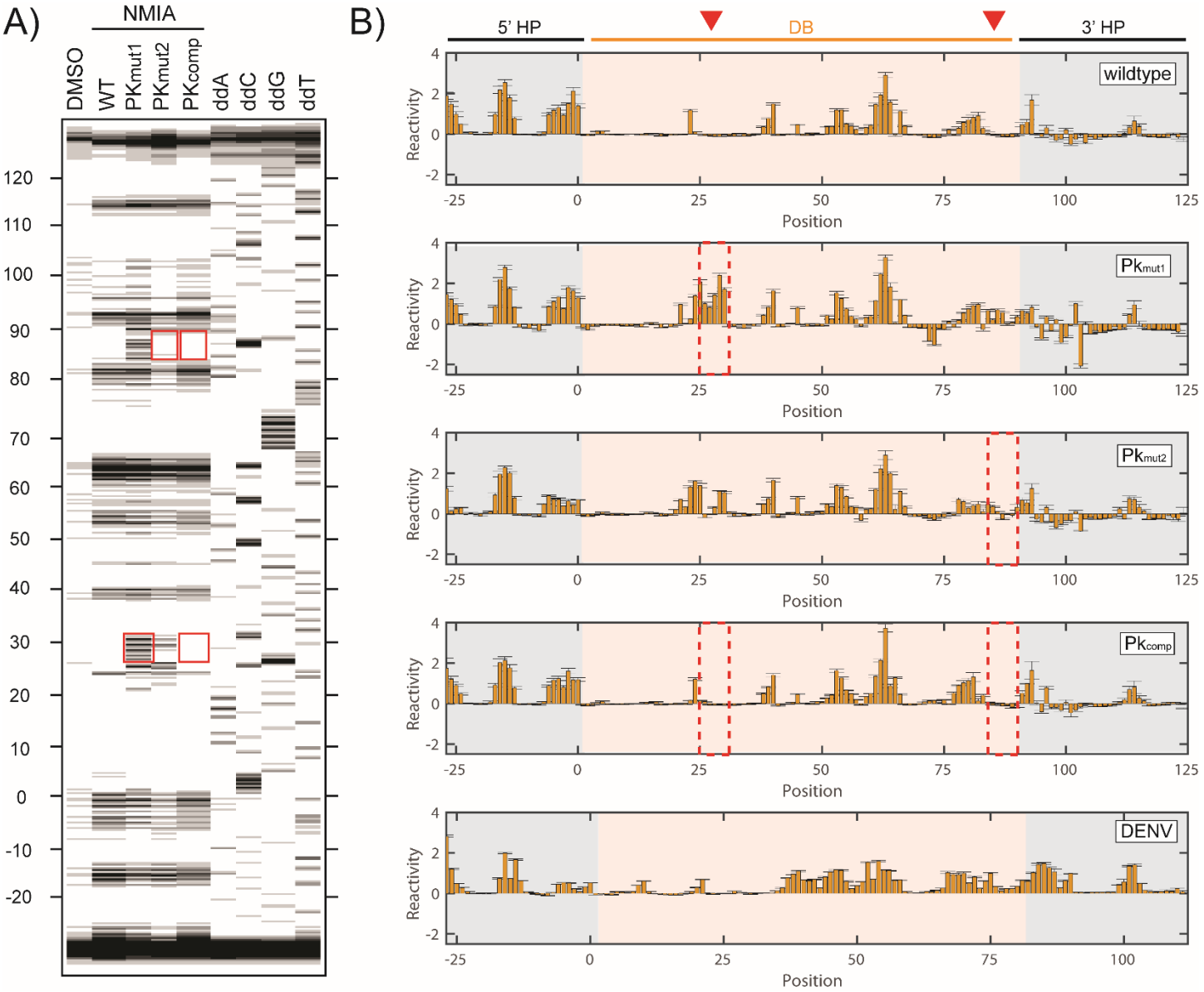

Suppl. Figure S7. Quantitation of NMIA chemical probing experiments. A) Capillary electropherogram of a reverse transcriptase reaction using DMSO- or NMIA-treated RNA for DONGV wildtype, PK_{mut1}, PK_{mut2}, and PK_{comp} constructs. Right lanes represent DONGV wildtype RNA treated with chain terminating nucleotides (ddATP, ddCTP, ddGTP, and ddTTP) to generate a reference ladder. Numbers indicate approximate nucleotide position, with the first nucleotide of the crystal structure set to 1. 5′ and 3′ hairpin extensions used for normalization are numbered (-27 to 0 and 91 to 125). Red boxes indicate the positions of mutations to the highlighted constructs. **B)** NMIA chemical probing quantitation for DONGV wildtype, PK_{mut1}, PK_{mut2}, and PK_{comp} DB constructs as well as the DENV-2 DB. Bars represent the difference in average reactivity from 4 replicate experiments between NMIA-treated RNA and a DMSO-treated control. Error bars = standard deviation. The position of the DB RNA within the construct is indicated in orange, as well as the position of 5′ and 3′ hairpins (HP) used for normalization and to confirm proper RNA folding in grey. Red triangles indicate the position of the pseudoknot and rex boxes indicate the positions of the mutations in that construct.

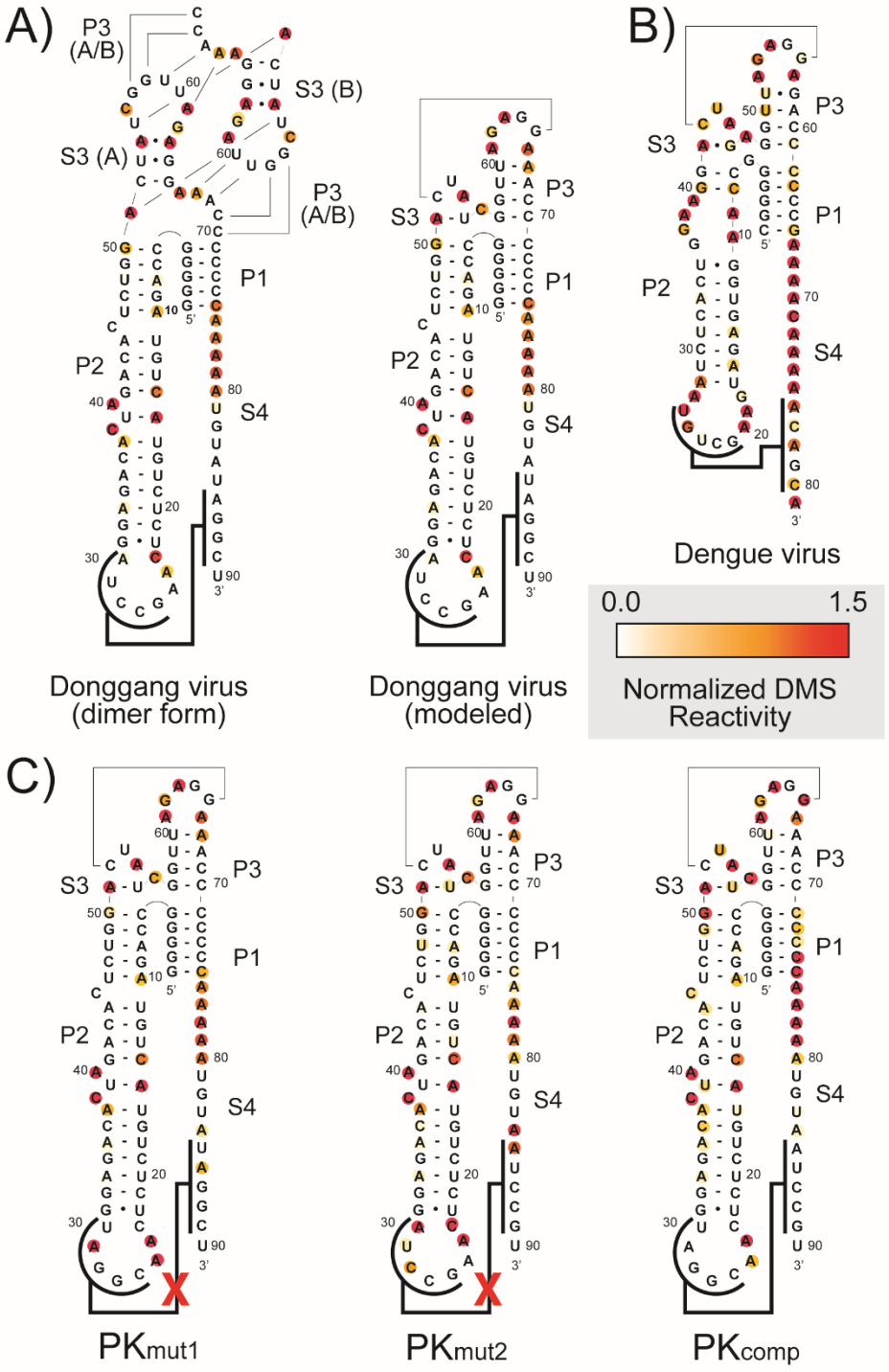

Suppl. Figure S8. DMS chemical probing of the DB RNA. Normalized DMS reactivity plotted against the secondary structure of A) DONGV DB crystal and modeled forms, B) DENV-2 DB, and C) DONGV pseudoknot mutants.

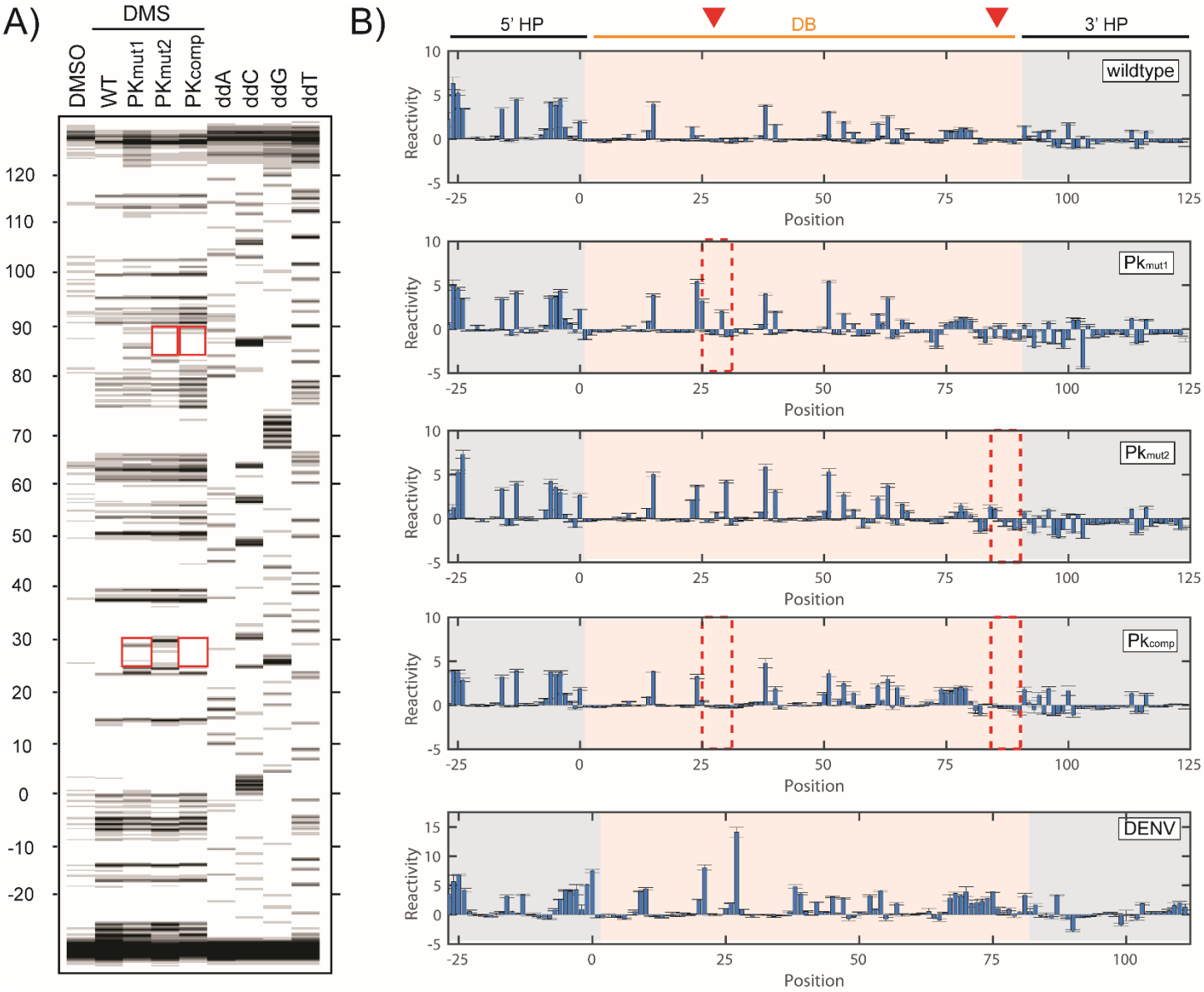

Suppl. Figure S9. Quantitation of DMS chemical probing experiments. A) Capillary electropherogram of a reverse transcriptase reaction using DMSO- or DMS-treated RNA for DONGV wildtype, PK_{mut1}, PK_{mut2}, and PK_{comp} constructs. Right lanes represent DONGV wildtype RNA treated with chain terminating nucleotides (ddATP, ddCTP, ddGTP, and ddTTP) to generate a reference ladder. Numbers indicate approximate nucleotide position, with the first nucleotide of the crystal structure set to 1. 5′ and 3′ hairpin extensions used for normalization are numbered (-27 to 0 and 91 to 125). Red boxes indicate the positions of mutations to the highlighted constructs. **B)** DMS chemical probing quantitation for DONGV wildtype, PK_{mut1}, PK_{mut2}, and PK_{comp} DB constructs as well as the DENV-2 DB. Bars represent the difference in average reactivity from 4 replicate experiments between DMS-treated RNA and a DMSO-treated control. Error bars = standard deviation. The position of the DB RNA within the construct is indicated in orange, as well as the position of 5′ and 3′ hairpins (HP) used for normalization and to confirm proper RNA folding in grey. Red triangles indicate the position of the pseudoknot and rex boxes indicate the positions of the mutations in that construct.

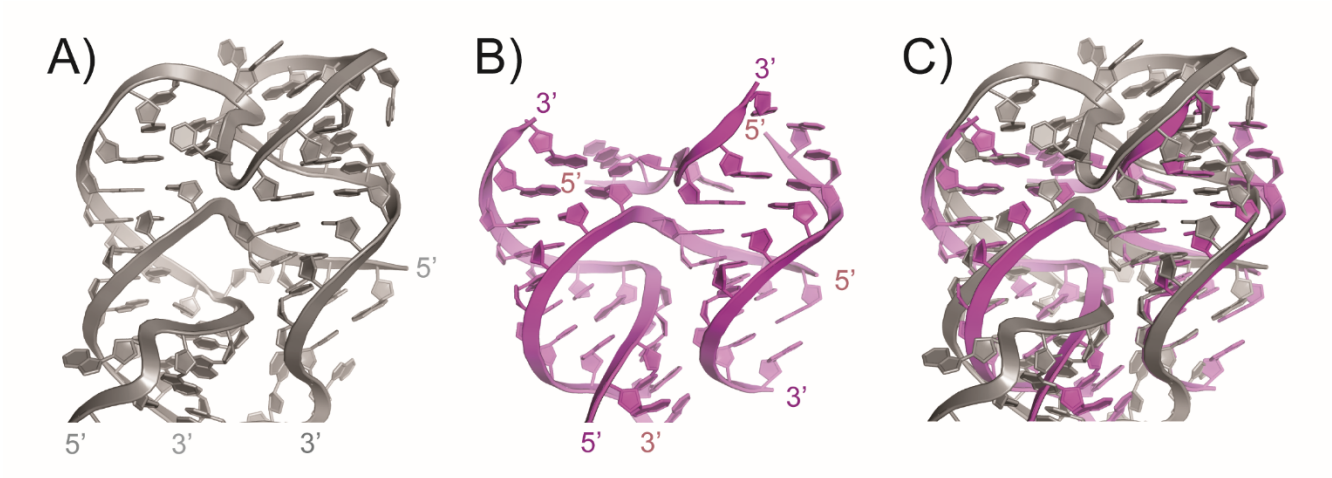

Suppl. Figure S10. Structural comparison of homologous four-way junctions. A) Four-way junction of the DONGV DB RNA. **B)** Four-way junction from RNase P (PDB ID: 1NBS) **C)** Structural superposition of (A) and (B).

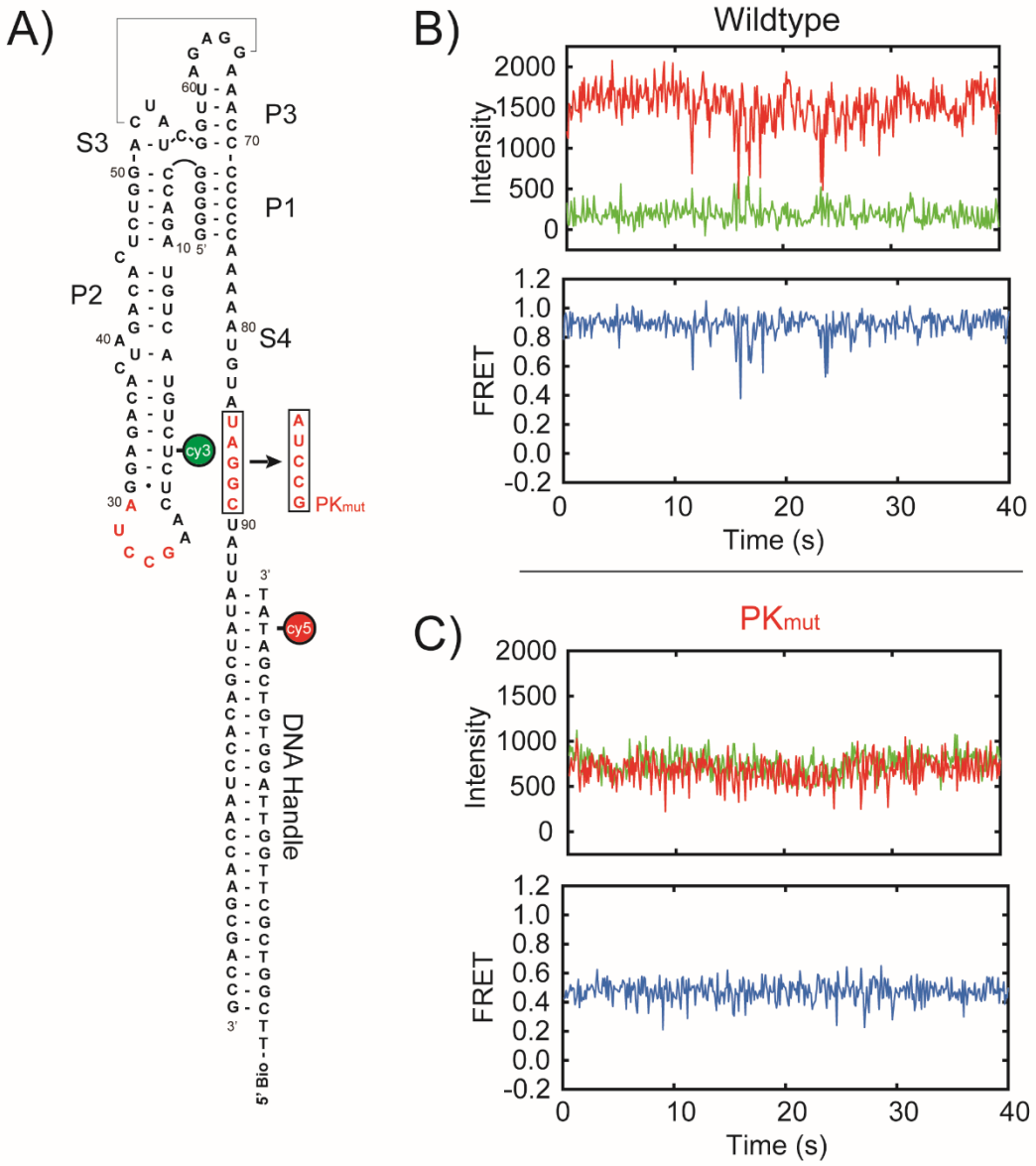

Suppl. Figure S11. Overview of smFRET experiments. A) Schematic of complete sequences used in smFRET experiment. Cy3 was site-specifically incorporated on residue U20 of the DONGV DB sequence and Cy5 was incorporated on the DNA handle. The DNA handle was modified with a 5′ biotin in order to immobilize the complex on a microscope slide by a biotin-streptavidin linkage. Pseudoknot residues are highlighted in red and the sequence of the pseudoknot mutant (PK_{mut}) is shown. **B)** Representative single molecule trace of a wildtype DONGV DB RNA. (Top) Intensity of Cy3 (green) and Cy5 (red) over time. (Bottom) Calculated FRET values over time. **C)** Representative single-molecule trace of the PK_{mut} construct showing Cy3 and Cy5 intensity and calculated FRET values as in B.

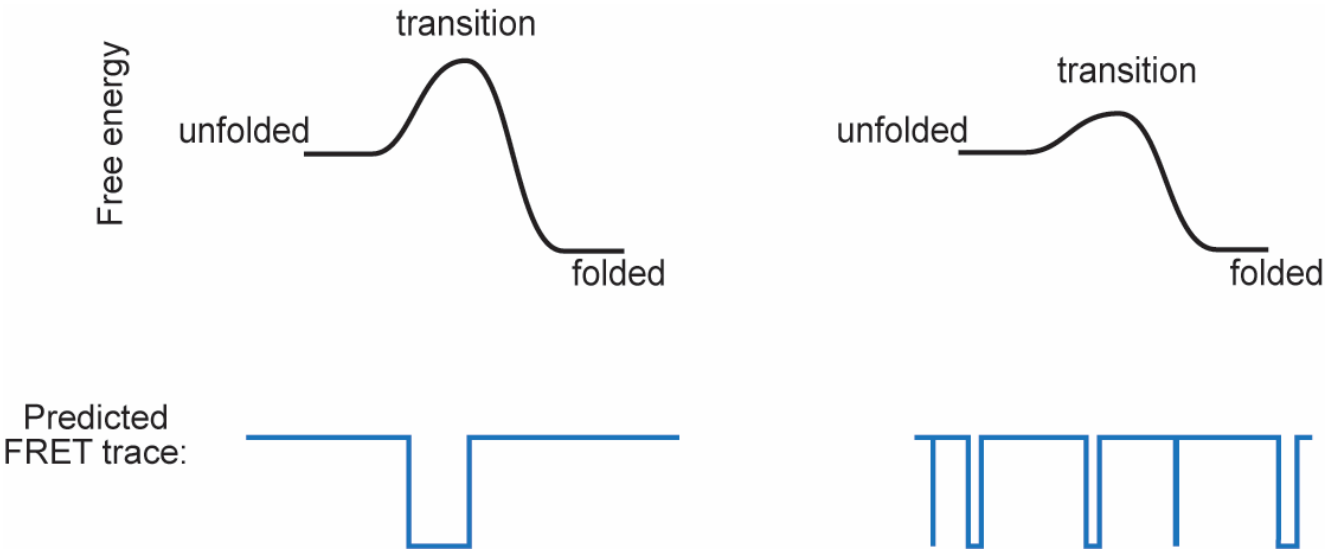

Suppl. Figure S12. Free energy landscapes and predicted smFRET trace values. A molecule with a high free energy to the transition state(left) will have long dwell times in the folded and unfolded states. A molecule with a lower free energy to the transition state (right) will have more frequent FRET changes with shorter dwell times. The FRET behavior of the DONGV DB RNA more closely resembles the example of the low free energy transition state. Note that the free energy difference between the folded and unfolded states remains the same in both cases, with the folded state predominating.

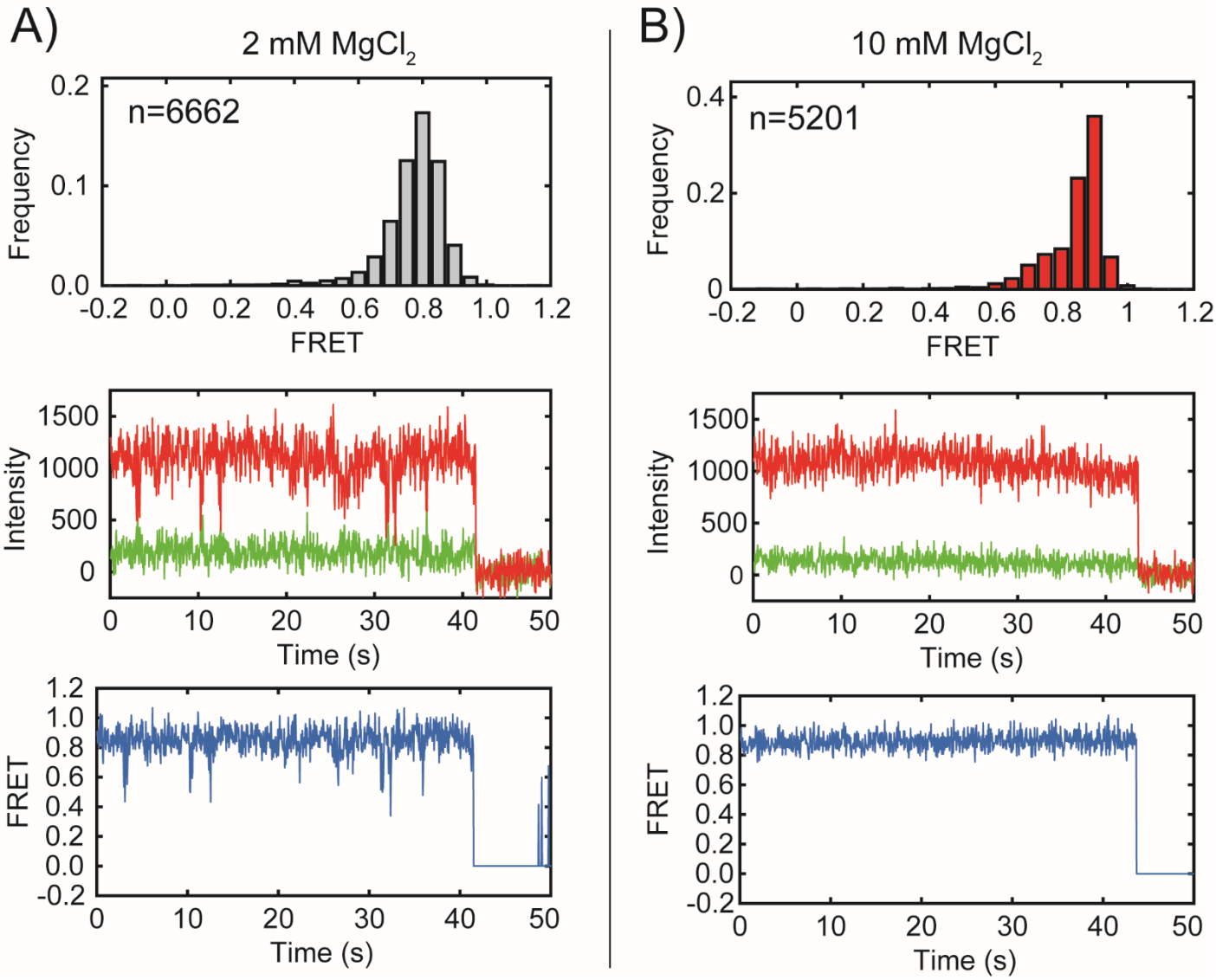

Suppl. Figure S13. Magnesium dependence of pseudoknot stability. A) Single-molecule histogram (top) of the FRET distribution of 6662 wildtype DONGV DB RNAs with dyes placed as in (Figure 7) in 2 mM $MgCl_2$. A representative single-molecule FRET trace following an individual molecule is below. The trace shows Cy3 (green) and Cy5 (red) intensity over time, with a calculated FRET trajectory (blue) displayed below. The loss of signal at the end of the trace is due to Cy3 photobleaching under laser illumination. **B)** Single-molecule histogram (top) of the FRET distribution of 5201 wildtype DONGV DB RNAs as in **(A)** but instead in 10 mM $MgCl_2$. A representative single-molecule FRET trace following an individual molecule is below and matches the scheme shown at left.

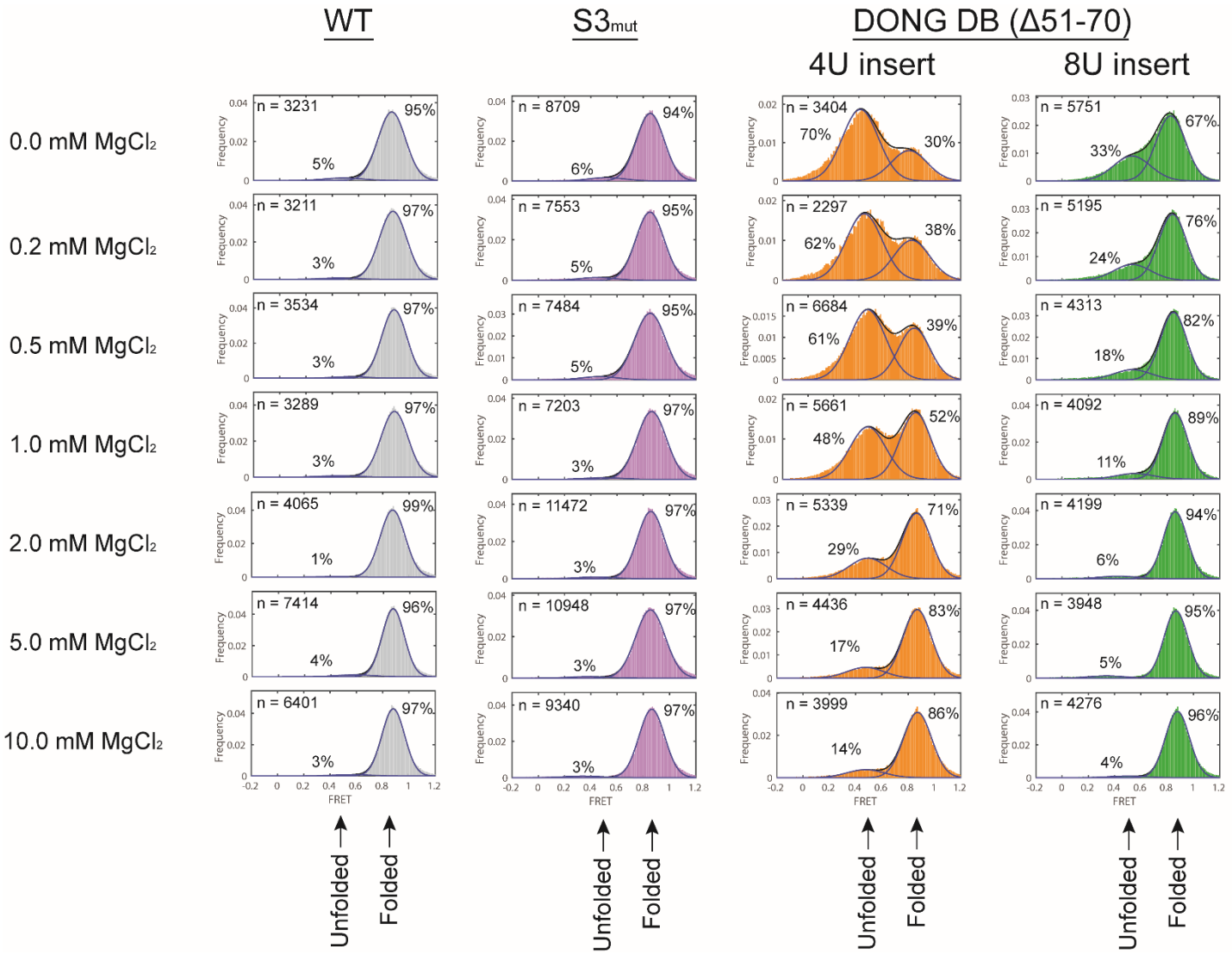

Suppl. Figure S14. Effect of $MgCl_2$ concentration on the folding of four-way junction mutants. smFRET histograms of Wildtype, $S3_{mut}$ (A51C/G65C), 8U insert, and 4U insert mutations tested at the indicated $MgCl_2$ concentrations. smFRET histograms were collected over 2 seconds at a 0.1 sec integration time to generate histograms of all FRET values observed during the observation window. Histograms were fit to the sum of two Gaussian distributions, with fits displayed on graph as well as the relative percentage of the pseudoknot unfolded (~0.5 FRET) and pseudoknot folded (~0.8 FRET) states as determined by the fit. The total number of molecules used to determine the smFRET histograms are listed in the upper left corner of the histogram. $MgCl_2$ concentration had little effect on the Wt and $S3_{mut}$ histograms, however it had a demonstrable effect on the 4U and 8U mutants. The fraction of the molecules in the folded states was used to determine the graph in Figure 8C.

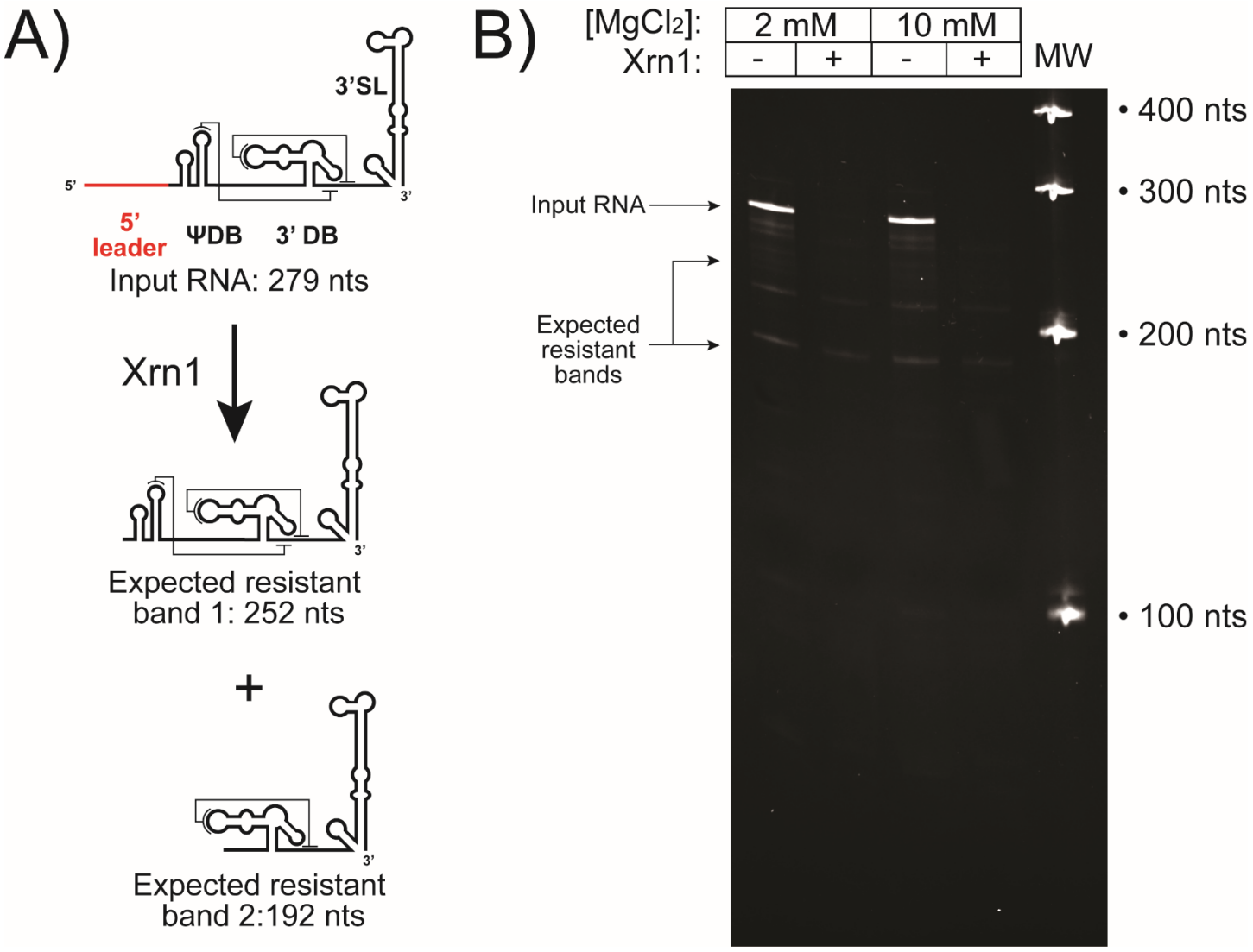

Suppl. Figure S15. XRN1 resistance of ΨDB and DB RNAs in the context of the 3' UTR. A) A ZIKV 3' UTR construct containing the ΨDB, DB, and 3' SL elements was *in vitro* transcribed with a single-stranded 5' leader for loading *K. lactis* Xrn1. The predicted sizes of potential ΨDB and DB XRN1-resistant products are shown. **B)** Ethidium bromide-stained denaturing PAGE gel of the input RNA treated with Xrn1 or left untreated at 2mM and 10 mM $MgCl_2$. A single-stranded molecular weight ladder is shown at the right. Arrows indicate the approximate migration point of 252 and 192 nt fragments. Although some weak staining RNA is visible in this region, it is present in all four lanes, suggesting a minor contaminant and not XRN1-resistant products.

Number of photobleaching events	Molecules observed
2+	39
1	311
0	455

Suppl. Table S1. Observed photobleaching events. Counting of double, single, and no photobleaching events observed in 160 second smFRET traces.

References for supplementary material:

1. de Borba, L., Villordo, S.M., Iglesias, N.G., Filomatori, C.V., Gebhard, L.G. and Gamarnik, A.V. (2015) Overlapping local and long-range RNA-RNA interactions modulate dengue virus genome cyclization and replication. *J Virol*, **89**, 3430-3437.